Print ISSN: 2321-6379
Online ISSN: 2321-595X

Original Article

Diagnostic Accuracy of Hounsfield Unit on Non Contrast Computed Tomography in Predicting Chemical Composition of Urinary Calculi

Padma V Badhe[1], Sanika Patil[2], Jagneet S Chatha[2], K N Puneethkumar[2]

[1]Professor, Department of Radiology, Seth Gordhandas Sunderdas Medical College, Mumbai, Maharashtra India, [2]Senior Resident, Department of Radiology, Seth Gordhandas Sunderdas Medical College, Mumbai, Maharashtra, India

Abstract

Introduction: Non-contrast computed tomography (NCCT) has become the imaging modality of choice for renal colic due to its high sensitivity in detecting renal stones. Predicting the chemical composition of renal stones based on radio-opacity can guide management strategies and therapeutic outcomes. The primary aim of our study was to evaluate the predictive efficacy of radio-opacity measures to accurately diagnose the chemical composition of the renal stones.

Methodology: NCCT of 250 consecutive adult patients were analyzed prospectively for whom chemical analysis of urinary stones was available over 18 months at an academic hospital in Western India. Multinomial univariate logistic regression was used to evaluate the predictive accuracy of radio-opacity measures - Hounsfield unit (HU) and Hounsfield density (HD). Data processing and multinomial logistic classifier training were done using a machine learning package in Python. Receiver operating characteristic (ROC) analysis was done using the R programming language.

Results: Calcium oxalate (61.2%) stones were the most common in our study populations, followed by Struvite (13.6%), calcium phosphate (13.2%), and uric acid (12%). Using ROC of uric acid versus struvite, HU provided a superior area under the curve (AUC) coverage of 100% compared to HD (AUC = 95.59%, CI95% = 91.23–99.95%), revealed by DeLong's test (Z = –1.9835, P = 0.047). Using the closest top-left method, an HU threshold of 731 (CI95% = 721–901%) with 100% specificity and 100% sensitivity. Similarly for struvite was predicted at 1136 HU versus calcium oxalate and phosphate stones with 76.47% specificity (CI95% = 64.71–88.24%) and 82.26% sensitivity (CI95% = 69.35–90.32%).

Conclusion: NCCT-based radio-opacity measures can identify uric acid from struvite, calcium stones in vivo with a high degree of accuracy at a threshold of 731 HU, and struvite from calcium oxalate and phosphate stones in vivo with a moderate degree of accuracy at a threshold of 1136 HU.

Key words: Chemical analysis of calculi, Non-contrast computed tomography, Renal stones/renal calculi, Urinalysis

INTRODUCTION

Ureteric colic caused by urolithiasis is an important and frequent emergency condition in medical practice. Approximately 5–12% of the world population will have a urinary tract stone during their lifetime with a 50% recurrence rate.[1] In the Indian scenario, recent estimates suggest a slightly elevated prevalence rate of 12–15% with a 50% recurrence rate of renal stones.[2] Non-contrast computed tomography (NCCT) has become the preferred imaging modality for the diagnosis of renal colic.[3] The American College of Radiology estimates a 98% diagnostic specificity of NCCT when a patient presents with acute flank pain suspicious of an obstructing stone.[4]

Access this article online

www.ijss-sn.com

Month of Submission : 11-2021
Month of Peer Review : 12-2021
Month of Acceptance : 12-2021
Month of Publishing : 01-2022

In addition to the size, location of the stone, and overall status of the kidney, there is increasing evidence for a correlation between the radio-opacities and chemical compositions of renal stones.[5-7] Predicting the chemical composition of renal stones based on radio opacity is important as their early identification can guide management strategies and therapeutic outcomes. For instance, uric acid stones can be treated by oral chemolysis, avoiding invasive therapies,

Corresponding Author: Dr. Padma V Badhe, Department of Radiology, Seth Gordhandas Sunderdas Medical College, Mumbai, Maharashtra, India.

while on the other hand, calcium oxalate stones are denser and less amenable to extra-corporeal shock wave lithotripsy (ESWL).[8,9] Dietary modifications are a very important part of the management of patients with renal stones and vary according to the composition of the stone.[10] Identification of chemical composition based on radio-opacity of stones on NCCT has shown promise in predicting the success and efficacy of ESWL and in the subsequent determination of appropriate medical management of renal stones.[5,7,11]

Since renal stones cannot always be obtained for chemical analysis, the need for accurate alternative methods for prediction of stone composition exists. Relatively few large stones are missed on NCCT but small stones (<3 mm) might slip between tissue imaging planes and evade detection.[12]

We carried out this study to assess the distribution of renal stones, to characterize them using radio-opacity measures, to evaluate the predictive efficacy of these measures toward the classification of chemical composition of the stones, and to identify optimal thresholds for classification. We sought to carry out robust statistical estimation and hypothesis testing for inference.

MATERIALS AND METHODS

The prospective observational study was carried out in the Department of Radiology, King Edward Memorial Hospital, Mumbai, India, over a period of 18 months from May 2016 to December 2018. An institutional ethics committee approval was obtained for the same. Patients were referred to us for computed tomography of kidney, ureters, and bladder (CT KUB) scan (KUB), and from these, a subset was included in the study for whom chemical composition analysis of stone was also carried out as per requests of referring clinicians. This included both out-patients as well as in-patients. Patients above 18 years of age were included in the study. Stones ≥10 mm were included in the study.

Scanning was performed as per standardized protocols for CT KUB scan. Each scan was interpreted by a professional radiologist, and radio-opacities of the stone (in Hounsfield units, HU) and the greatest transverse diameter of the stone was measured in millimeters. HU were calculated by drawing a circular region-of-interest mask over the two-third area of each stone. The transverse diameter was taken by measuring the maximum dimension of the calculus. Hounsfield density (HD) was calculated as the ratio of HU over the greatest transverse diameter in millimeters.

Chemical analysis of the stone was performed and evaluated in groups as calcium oxalate and phosphate, uric acid, and struvite stones. CT scan data were obtained with following parameters: Field of view: 350 mm, Slice thickness: 2 mm, Increment: 1 mm, Filter: Standard (B), Window: C: 60 W: 360 modifiable, and Matrix: 512, Pitch: 1.5:1.

Descriptive statistics are presented as 20% trimmed means and bootstrapped 95% confidence intervals, which are robust estimates of the underlying distribution.[13] Normality tests were carried out using the Shapiro–Wilk test. Hypothesis testing was done using a bootstrapped robust analysis of variance (ANOVA), which tests the null hypothesis for equal 20% trimmed means across groups.[13] All bootstrap-based methods involved 10,000 iterations of resampling.

The predictive efficiency of radio-opacity measures was evaluated through multinomial univariate logistic regression. This was carried out separately for HU and HD each after carrying out recursive feature elimination for feature ranking with three-fold cross-validation. Optimization for the logistic regression model fitting was done using the L-BGFS algorithm to minimize cross-entropy loss regularized by the L2 penalty. Diagnostics for the model fit are presented in the form of classification performance, predicted probabilities, log-loss or cross-entropy loss, and Matthew's correlation coefficient (MCC).[14]

Data processing and multinomial logistic classifier training were done using pandas[15] and scikit-learn[16] machine learning package in Python. Robust estimation and hypothesis testing were carried out using the Wilcox' Robust Statistics package,[13,17] Receiver operating characteristic (ROC) analysis was carried out using the predictive ROC (pROC) package by Robin *et al.*,[18] plotting was done using Wickham[19] and Wilke *et al.*[20] packages for the R programming language.[21]

RESULTS

Renal stone analysis of the 250 patients included in the study revealed a highest proportion of calcium oxalate (61.2%), followed by struvite (13.6%), calcium phosphate (13.2%), and uric acid (12%). The proportions of chemical composition, presented in Table 1, did not differ significantly across gender ($\chi^2 = 0.110$, $P = 0.993$, 104 Monte Carlo simulations). Ages ranged from 20 to 55 (Mean 20% trim = 39.64, SE = 1.66), and did not differ significantly across chemical compositions (F3,

Table 1: Contingency tables–chemical compositions across sex

Sex	Chemical Composition				Total
	Uric acid	Struvite	Oxalate	Phosphate	
Female	13	16	68	15	112
Male	17	18	85	18	138
Total	30	34	153	33	250

χ^2=0.110 (p_{sim}=0.993, based on 10,000 Monte Carlo simulations)

42.42 = 0.884, $P = 0.476$). Maximum measured dimensions across the stone ranged from 1.2 cm to 2.6 cm (Mean 20% trim = 1.86, SE = 0.07), and also did not differ across chemical compositions (F3, 45.13 = 2.869, $P = 0.0538$).

The distributions of radio-opacity measures –HD and HU, summarized in Table 2, were non-normal. Separate robust one-way ANOVA tests for HD and HU across chemical compositions, presented in Table 3, estimated significant statistics with relatively large effect sizes. Pairwise bootstrapped robust *post hoc* tests revealed significant differences between all pairs of chemical compositions for both measures except for differences in HD between calcium oxalate and calcium phosphate, summarized in Table 4 and Figure 1.

To assess the predictive efficiency of the radio-opacity measures, multinomial univariate logistic classifiers were trained separately on HD and HU for the chemical composition classes – uric acid, struvite, and calcium (oxalate and phosphate combined). For HD, model fitting converged in 43 iterations achieving overall classification accuracy of 85.2%, with cross-entropy loss of 0.394 and MCC of 0.613. For HU, model fitting converged in 76 iterations achieving overall classification accuracy of 89.2%, with cross-entropy loss of 0.279 and MCC of 0.726. Classifier performance for both HD and HU is summarized in Table 5 and class predictions for chemical compositions are presented in Figure 2.

ROC curve estimation was carried out for estimation of discrimination thresholds in the binary classification of uric acid–struvite and struvite–calcium using HD and HU. The pROC package for R was used for the analysis and estimation of bootstrapped thresholds and performance metrics. For multi-class ROC, area under the curve (AUC) was estimated to be 91.88% for HD and 94.71% for HU.

For binary classification of uric acid versus struvite, HU provided a superior AUC coverage of 100% compared to HD (AUC = 95.59%, CI95% = 91.23–99.95%), revealed by DeLong's test (Z = –1.9835, $P = 0.047$). Using the closest top-left method, an HU threshold of 731 (CI95% = 721–901%) with 100% specificity and 100% sensitivity, performed better than a HD threshold of 46 (CI95% = 40–48%) with 91.18% specificity (CI95% = 82.35–100%), and 90% sensitivity (CI95% = 80–100%).

For binary classification of struvite versus calcium, HU provided a AUC coverage of 84.14% (CI95% = 76.64–91.64%) while HD provided coverage of 80.76% (CI95% = 73.44–88.07%), with no differences in AUC as revealed by DeLong's test (Z = 0.687, $P = 0.492$). Using the closest top-left method, a HU threshold of 1136 (CI95% = 1092.5–1208.5%) with 76.47% specificity (CI95% = 64.71–88.24%) and 82.26% sensitivity (CI95% = 69.35–90.32%), performed better than an HD threshold of 63.5 (CI95% = 59.5–70.5%) with 76.47% specificity (CI95% = 61.76–94.12%) and 73.66% sensitivity (CI95% = 55.91–87.63%). Estimates using Youden's J statistic were very similar to the ones obtained using the closest top-left method. Estimated ROC curves are presented in Figure 3, while performance estimates of discrimination thresholds are summarized in Figure 4.

DISCUSSION

Our findings demonstrate significant differences in radio-opacity measures both – normalized over the greatest transverse

Table 2: Characterization of NCCT-based radio-opacity measures across chemical compositions of renal calculi

Measure	Estimate	Overall	Uric acid	Struvite	Oxalate	Phosphate
Hounsfield Density	Mean±SE†	73.12±1.67	33.63±1.73	59.26±2.06	79.18±1.63	95.24±5.45
	20% Trimmed Mean±SE†	70.85±1.63	33.05±2.08	58.86±2.30	76.54±1.82	92.67±7.47
	Median±SE†	68.50±1.64	32.50±2.52	58.50±3.13	75.00±1.91	85.00±12.04
	Minimum	18.00	18.00	36.00	27.00	50.00
	Maximum	156.00	55.00	90.00	136.00	156.00
	5th Percentile	30.00	19.10	39.75	54.00	52.80
	95th Percentile	122.10	52.25	81.00	117.6	144.80
	Shapiro–Wilk (W)	0.976	0.973	0.980	0.961	0.916
	Shapiro–Wilk (*P*)	<0.001*	0.616	0.760	<0.001*	0.014*
Hounsfield Units	Mean±SE†	1179.06±18.32	566.80±15.54	1064.12±26.55	1273.03±18.32	1418.36±33.62
	20% Trimmed Mean±SE†	1218.51±16.87	564.55±21.49	1052.68±25.66	1271.01±14.99	1425.95±43.32
	Median±SE†	1215.50±15.79	557.00±23.55	1030.00±31.95	1276.00±18.32	1439.00±43.25
	Minimum	420.00	420.00	760.00	908.00	1045.00
	Maximum	1722.00	702.00	1433.00	1658.00	1722.00
	5th Percentile	544.80	451.95	813.00	995.20	1096.00
	95th Percentile	1563.65	700.00	1357.60	1560.00	1686.80
	Shapiro–Wilk (W)	0.937	0.936	0.968	0.990	0.950
	Shapiro–Wilk (*P*)	<0.001*	0.073	0.405	0.347	0.137

†SE indicates the bootstrapped Standard Error of the estimate based on 10,000 iterations, NCCT: Non-contrast computed tomography

diameter of the stone (HD) as well as for unnormalized (HU), across chemical compositions of renal stones. Among reports involving radio-opacities of renal stones in Indian populations, HU estimates from our sample were higher for uric acid (420–702 vs. 200–450), lower for struvite (760–1433 vs. 600–900), and calcium oxalate (908–1658 vs. 1700–2800) and similar for calcium phosphate (1045–1722 vs. 1200–1600).[22] Compared to another study in the Indian setting,[23] HU estimates from our sample were higher for struvite (760–1433 vs. 486–1169) and calcium oxalate (908–1658 vs. ~258–1447), and similar for uric acid (420–702 vs. 433–634).

Table 3: Robust ANOVA†: HD and HU across chemical compositions

Measure	df1	df2#	F	*P*	ξ‡
HD	3	46.85	77.480	<0.001*	0.900
HU	3	43.92	243.819	<0.001*	0.841

†Tests hypothesis of equal trimmed means using the bootstrap-t method with 10,000 iterations; #Estimated adjusted degrees of freedom; ‡Explanatory measure of effect size, HD: Hounsfield density, HU: Hounsfield units, ANOVA: Analysis of variance

We found uric acid stones to have the lowest HD and HU measures followed by struvite and calcium stones. The predictive performance of HU exceeded that of HD for the classification of chemical compositions, with better performing thresholds for discrimination of uric acid from struvite than calcium from struvite. We observed that uric acid stones were differentiated easily from the rest using HU with a very high degree of accuracy, while differentiation of calcium from struvite stones was only moderately accurate.

Predicting the chemical compositions of renal stones is vital for their management and treatment outcomes. ESWL is largely prohibitive for uric acid stones due to their relative fragility. On the other hand, calcium containing stones, notably oxalate monohydrate, are denser and more resistant to ESWL. Marks and Teichman,[24] 2007, have reported on the efficacy of Holmium laser as a function of chemical composition, wherein they observed a low susceptibility for fragmentation in the case of calcium oxalate monohydrate stones, and a moderate susceptibility for fragmentation of uric acid and

Table 4: Robust *post hoc* comparisons for HD and HU across chemical compositions of renal calculi

Measure	Comparison	Test statistic	SE†	*P*	p_{FDR}#	ψ‡	CI_{Lower}	CI_{Upper}
Hounsfield Density (HD)	Oxalate–Phosphate	–2.061	7.82	0.054	0.054	–16.13	–37.65	5.39
	Oxalate–Struvite	6.020	2.94	<0.001*	<0.001*	17.67	9.60	25.75
	Oxalate–Uric acid	14.834	2.931	<0.001*	<0.001*	43.48	35.42	51.54
	Phosphate–Struvite	4.259	7.94	0.001*	0.002*	33.80	11.98	55.63
	Phosphate–Uric acid	7.513	7.93	<0.001*	<0.001*	59.61	37.79	81.43
	Struvite–Uric acid	8.019	3.22	<0.001*	<0.001*	25.81	16.96	34.66
Hounsfield Units (HU)	Oxalate–Phosphate	–3.143	49.29	0.007*	0.007*	–154.94	–295.01	–14.87
	Oxalate–Struvite	7.223	30.23	<0.001*	<0.001*	218.33	132.44	304.22
	Oxalate–Uric acid	26.345	26.82	<0.001*	<0.001*	706.45	630.26	782.65
	Phosphate–Struvite	6.932	53.85	<0.001*	<0.001*	373.27	220.26	526.28
	Phosphate–Uric acid	16.561	52.01	<0.001*	<0.001*	861.40	713.61	1009.19
	Struvite–Uric acid	14.156	34.48	<0.001*	<0.001*	488.13	390.15	586.11

†Bootstrapped Standard Error of the test statistic and ‡bootstrapped robust estimate of the difference based on 10,000 iterations; #*P*-values adjusted for control of Family-wise Error Rate using Bonferroni correction, HD: Hounsfield density, HU: Hounsfield units

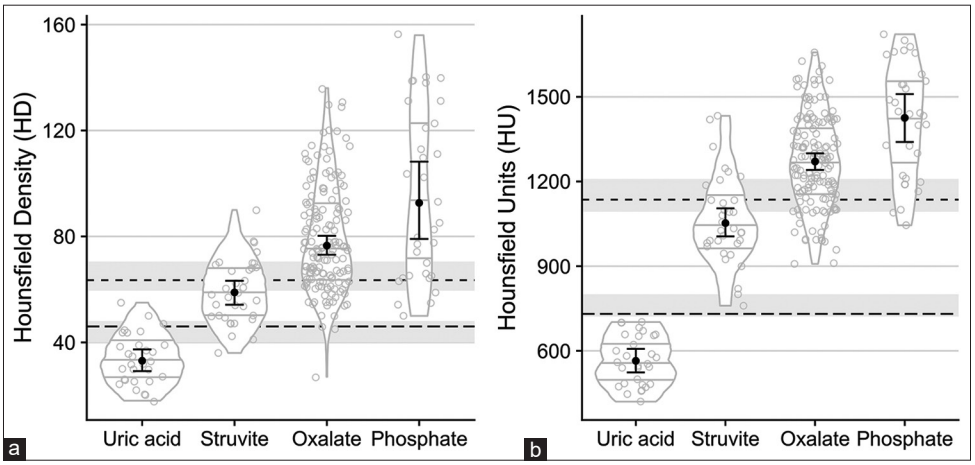

Figure 1: Distribution of Hounsfield Density (a) and Hounsfield Units (b) across chemical compositions. Point estimate represents the 20% trimmed mean, and the interval estimate represents the bootstrapped 95% confidence interval adjusted for control of the Family Wise Error Rate. Dashed lines represent the estimated thresholds for classification, and the gray band surrounding them represents the bootstrapped 95% confidence interval

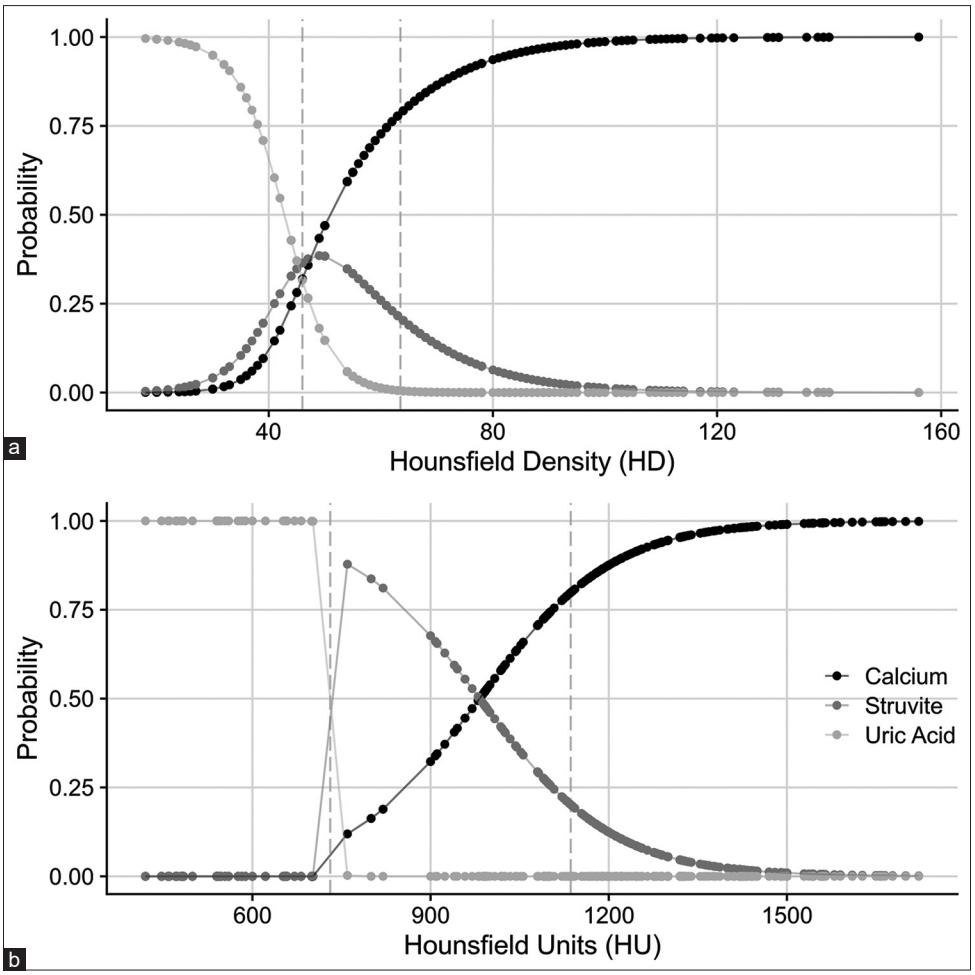

Figure 2: Probabilities predicted for observed samples by the multinomial logistic classifier using Hounsfield density (a), Hounsfield units (b). Vertical dashed lines indicate estimated thresholds

Table 5: Multinomial logistic regression† performance

Composition	Precision (%)	Sensitivity (%)	Specificity (%)	F_1 score‡ (%)
Hounsfield Density				
Calcium	85.92	98.39	53.13	91.73
Struvite	60.00	8.82	99.07	15.38
Uric acid	84.38	90.00	97.72	87.10
$Mean_{Weighted}$	82.21	85.20	64.73	80.79
Hounsfield Units				
Calcium	88.41	98.39	62.50	93.13
Struvite	76.92	29.41	98.61	42.55
Uric acid	100.00	100.00	100.00	100.00
$Mean_{Weighted}$	88.24	89.20	71.91	80.79

†L_2 penalized model that minimizes cross-entropy loss, learnt using a L-BGFS solver in 43 (HD) and 76 (HU) iterations; ‡F_1 score is the harmonic mean of precision and sensitivity, HD: Hounsfield density, HU: Hounsfield units

cystine stones. Uric acid has a solubility of ~50% at urinary pH of 5.75, while it is nearly completely soluble at urinary pH of 7. Precipitation of uric acid at low urinary pH predisposes patients to uric acid stones, thereby rendering non-invasive therapies like urine alkalinization a viable therapeutic strategy. Thus, separating uric acid stones from stones with other chemical compositions is critical. Both struvite and calcium stones are associated with urinary tract infections, with a higher risk of post-treatment sepsis and recurrence. Identification of these stones *in vivo* may help in directing appropriate therapy well in advance of stone extraction.

The present study was a single-center prospective effort, with a potential for selection bias. We believe that our usage of resampling methods and robust statistics would have addressed crucial statistical issues due to imbalanced

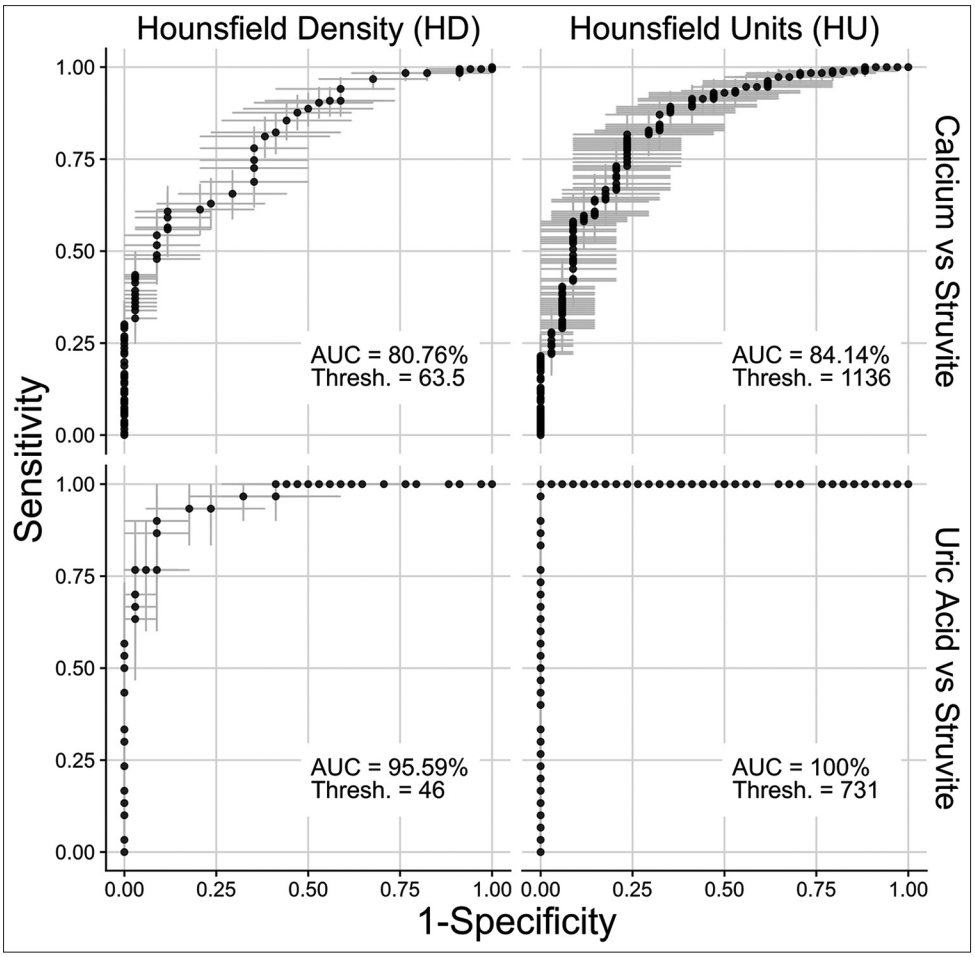

Figure 3: Receiver operating characteristic curve for Hounsfield density and Hounsfield units for binary classification of uric acid versus struvite and calcium versus struvite. Gray hatched lines indicate the bootstrapped 95% confidence interval for sensitivity and specificity

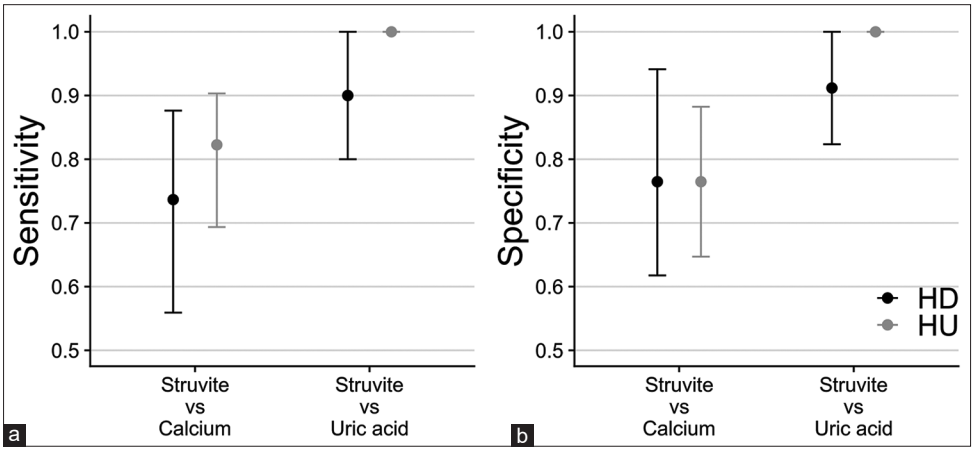

Figure 4: Performance of discrimination thresholds estimated from receiver operating characteristic curves. Point estimates indicate sensitivity and specificity at the estimated thresholds, while interval estimates indicate bootstrapped 95% confidence intervals. No intervals estimated for thresholds with 100% sensitivity and specificity

sample sizes within chemical compositions; however, the extent of this reduction cannot be determined. We did not encounter any cysteine, brushite, or hydroxyapatite stones. Furthermore, given the design of the study, we could not assess the impact of stone composition detection using NCCT on patient management and outcomes. We could not assess stone density, which may complement heterogeneity indices and offer reliable predictive performance. Finally,

we did not carry out statistical inference on the trained multinomial logistic classifier due to difficulties presented by regularization and given our aim of univariate model selection for prediction accuracy.

CONCLUSIONS

NCCT-based radio-opacity measurement can identify uric acid from struvite, calcium oxalate, and phosphate stones *in vivo* with a high degree of accuracy at a threshold of 731 HU, and struvite from calcium oxalate and phosphate stones *in vivo* with a moderate degree of accuracy at a threshold of 1136 HU. Using pooled datasets, additional predictors and robust techniques, a higher and more reliable predictive performance are achievable, with immense scope for facilitation of management strategies.

ACKNOWLEGMENT

The authors express their gratitude to the Department of Radiology of, Seth G.S Medical College and KEM Hospital, Mumbai, for providing the required platform to complete this Original Research Article. The authors express their gratitude to their colleagues for valuable suggestions regarding the article. Finally, the authors are thankful to the patient without whose help it would not have been possible to complete the article. The authors have not declared a specific grant for this research from any funding agency in the public, commercial, or not-for-profit sectors.

REFERENCES

1. Masarani M, Dinneen M. Ureteric colic: New trends in diagnosis and treatment. Postgrad Med J 2007;83:469-72.
2. Gupta S, Baghel MS, Bhuyan C, Ravishankar B, Ashok BK, Patil PD. Evaluation of anti-urolithiatic activity of Pashanabhedadi Ghrita against experimentally induced renal calculi in rats. AYU 2012;33:429.
3. Feroze S, Singh B, Gojwari T, Manjeet S, Athar B, Hamid H. Role of non-contrast spiral computerized tomography in acute ureteric colic. Indian J Urol 2007;23:119.
4. Brisbane W, Bailey MR, Sorensen MD. An overview of kidney stone imaging techniques. Nat Rev Urol 2016;13:654-62.
5. El-Assmy A, El-Nahas AR, Abou-El-Ghar ME, Awad BA, Heir KZ. Kidney stone size and hounsfield units predict successful shockwave lithotripsy in children. Urology 2013;81:880-4.
6. Gücük A, Üyetürk U. Usefulness of Hounsfield unit and density in the assessment and treatment of urinary stones. World J Nephrol 2014;3:282-6.
7. Yamashita S, Kohjimoto Y, Iwahashi Y, Iguchi T, Nishizawa S, Kikkawa K, *et al*. Noncontrast computed tomography parameters for predicting shock wave lithotripsy outcome in upper urinary tract stone cases. BioMed Res Int 2018;2018:e9253952.
8. Williams JC, Saw KC, Paterson RF, Hatt EK, McAteer JA, Lingeman JE. Variability of renal stone fragility in shock wave lithotripsy. Urology 2003;61:1092-6.
9. Ringdén I, Tiselius HG. Composition and clinically determined hardness of urinary tract stones. Scand J Urol Nephrol 2007;41:316-23.
10. Prezioso D, Strazzullo P, Lotti T, Bianchi G, Borghi L, Caione P, *et al*. Dietary treatment of urinary risk factors for renal stone formation. A review of CLU Working Group. Arch Ital Urol Androl 2015;87:105.
11. Ouzaid I, Al-Qahtani S, Dominique S, Hupertan V, Fernandez P, Hermieu JF, *et al*. A 970 Hounsfield units (HU) threshold of kidney stone density on non-contrast computed tomography (NCCT) improves patients' selection for extracorporeal shockwave lithotripsy (ESWL): Evidence from a prospective study. BJU Int 2012;110:E438-42.
12. Memarsadeghi M, Heinz-Peer G, Helbich TH, Schaefer-Prokop C, Kramer G, Scharitzer M, *et al*. Unenhanced multi-detector row CT in patients suspected of having urinary stone disease: Effect of section width on diagnosis. Radiology 2005;235:530-6.
13. Wilcox RR. Introduction to Robust Estimation and Hypothesis Testing. 4th ed. Waltham, MA: Elsevier; 2016.
14. Baldi P, Brunak S, Chauvin Y, Andersen CA, Nielsen H. Assessing the accuracy of prediction algorithms for classification: An overview. Bioinformatics 2000;16:412-24.
15. Reback J, McKinney W, Van den Bossche J, Augspurger T, Cloud P, Klein A, *et al*. Pandas-dev/Pandas: Pandas 1.2.2. United Kingdom: Zenodo; 2021.
16. Pedregosa F, Varoquaux G, Gramfort A, Michel V, Thirion B. Scikit-learn: Machine learning in python. J Mach Learn Res 2011;12:2825-30.
17. Mair P, Wilcox R. Robust statistical methods in R using the WRS2 package. Behav Res 2020;52:464-88.
18. Robin X, Turck N, Hainard A, Tiberti N, Lisacek F, Sanchez JC. pROC: An open-source package for R and S+ to analyze and compare ROC curves. BMC Bioinform 2011;12:77.
19. Wickham H. ggplot2: Elegant Graphics for Data Analysis. New York: Springer-Verlag; 2016. Available from: https://www.ggplot2.tidyverse.org [Last accessed on 2020 Nov 23].
20. Wilke C, Fox SJ, Bates T, Manalo K, Lang B, Barrett M, Stoiber M, *et al*. Wilkelab/Cowplot: 1.1.1. United Kingdom: Zenodo; 2021.
21. R Core Team. R: A Language and Environment for Statistical Computing. Vienna, Austria: R Foundation for Statistical Computing; 2018. Available from: https://www.R-project.org [Last accessed on 2020 Nov 23].
22. Naik D, Jain A, Hegde AA, Kumar AA. Determination of attenuation values of urinary calculi by non-contrast computed tomography and correlation with outcome of extracorporeal shock wave lithotripsy-a prospective study. Int J Anat Radiol Surg 2017;6:81-6.
23. Mahalingam H, Lal A, Mandal AK, Singh SK, Bhattacharyya S, Khandelwal N. Evaluation of low-dose dual energy computed tomography for *in vivo* assessment of renal/ureteric calculus composition. Korean J Urol 2015;56:587-93.
24. Marks AJ, Teichman JM. Lasers in clinical urology: State of the art and new horizons. World J Urol 2007;25:227-33.

How to cite this article: Badhe PV, Patil S, Chatha JS, Puneethkumar KN. Diagnostic Accuracy of Hounsfield Unit on Non Contrast Computed Tomography in Predicting Chemical Composition of Urinary Calculi. Int J Sci Stud 2022;9(10):89-95.

Source of Support: Nil, **Conflicts of Interest:** None declared.